Behaviour of aluminium oxide in $KF-AlF_3-Al_2O_3$ melts and suspensions

Andrey S. Yasinskiy[1*], Andrey V. Suzdaltsev[2], Peter V. Polyakov[1], Sai Krishna Padamata[1], Olga V. Yushkova[1]

[1] *School of non-ferrous metals and materials science, Siberian federal university, Krasnoyarsk, Russia*

[2] *Institute of High-Temperature Electrochemistry UB RAS, Yekaterinburg, Russia*

**Corresponding author, e-mail: ayasinskiykrsk@gmail.com*

Abstract

The article addresses the properties of melts and alumina suspensions based on the molten $KF-AlF_3-Al_2O_3$ system, the kinetics of alumina dissolution and the rheological properties that determine the sedimentation stability. The study of such suspensions has become topical due to the prospects of their use as electrolytes in the production of aluminium using carbon-free anodes. The effects of the temperature, the particle size and the phase composition of the dispersed material and its volume fraction in the suspension on the dissolution kinetics and the sedimentation velocity are studied. The experiments were carried out over the melts with cryolite ratios 1.3 and 1.5 in the range of 750-850 °C. Three different types of aluminium oxide were used. The Reynolds numbers for sedimentation have indicated the Stokesian regime. Typical alumina dissolution rates were in the range 0.028-0.167 $g \cdot kg^{-1} \cdot s^{-1}$, which is close to the values reported previously. Sedimentation velocities were in the range $(0.05-3.61) \cdot 10^{-2}$ m/s, which is several times higher than those obtained previously for 700 °C and φ = 0.24-0.32. It is shown that mechanical activation of alumina increases the performance of the suspension in terms of the sedimentation stability and the dissolution rate increasing.

Keywords: dissolution rate, alumina, mechanical activation, low-temperature electrolyte, aluminium production, suspension, molten salt.

Introduction

The Hall-Heroult process has been used for decades for primary aluminium production at 960 °C with consumable carbon anodes and it has been a while since the alternative lower-temperature technologies started to be developed [1]. The dissolution of alumina is the critical process in both commercial $NaF-AlF_3-CaF_2$ and low-temperature $KF-AlF_3$ melts.

The reasons for the attention paid to molten $KF-AlF_3$ systems are as follows [2]:

- the liquidus temperature of this system is much lower (560 °C at $[AlF_3] \approx 45$ mol.%) than that of $NaF-AlF_3$;
- alumina solubility in pure potassium cryolite is 30% higher than that of sodium cryolite.

The mentioned advantages make it possible to replace carbon anodes with metallic, ceramic or cerametallic ones, which enable oxygen evolution instead of greenhouse gases (CO, CO_2, COF_2, CF_4,

C_2F_6, etc.). Several disadvantages have also appeared while using potassium salts instead of sodium ones. Electrical conductivity is lower, which increases energy requirements. Another issue is that potassium interacts with carbon-based cathodes and lining parts that makes it rather impossible to use them.

A decrease in the electrolyte temperature increases the corrosion resistance of oxygen-evolving anodes but reduces the alumina solubility and dissolution rate. It makes it more difficult to operate the electrolysis cell. The so-called sludges (undissolved alumina trapped under the liquid aluminium in the cell) are formed, and catastrophic corrosion of the anode may take place.

The dissolution mechanism and kinetics in sodium cryolite are studied and reported elsewhere [3-7]. Alumina is believed to be dissolved in the commercial electrolyte by one or several of the following mechanisms [8, 9]:

$$Al_2O_3 + 4AlF_5^{2-} + 4F^- \rightarrow 3Al_2OF_8^{4-} \quad (1)$$

$$Al_2O_3 + 4AlF_5^{2-} \rightarrow 3Al_2OF_6^{2-} + 2F^- \quad (2)$$

$$Al_2O_3 + AlF_5^{2-} + F^- \rightarrow {}^3/_2\, Al_2O_2F_4^{2-} \quad (3)$$

$$2Al_2O_3 + Al_2O_2F_4^{2-} + 4F^- \rightarrow 2Al_3O_4F_4^{3-} \quad (4)$$

The mechanism should not be changed drastically with the replacement of sodium cryolite with the potassium one. However, the kinetics is highly affected by electrolyte composition, temperature and hydrodynamic conditions and is poorly covered in the literature [10].

Suspension electrolytes were proposed to increase corrosion resistance and cathodic metal purity [11-14]. The schematic representation of the suspension electrolysis technology is shown in Fig. 1. The rheological (sedimentation velocity, maximum packing fraction) and electrochemical behaviour of these suspensions become an important field to study [15-20].

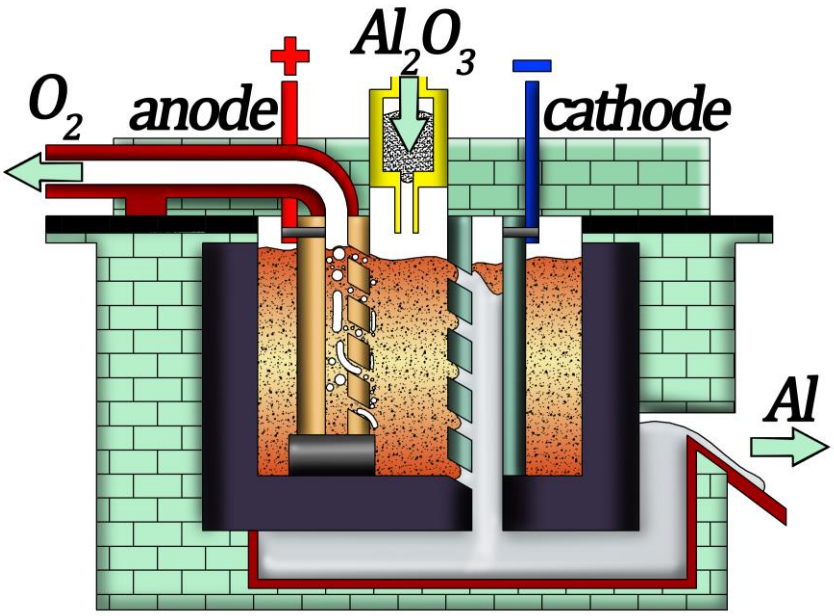

Fig. 1 – The scheme of suspension electrolysis apparatus

Determining the dissolution rate of alumina in melts has great importance as it influences the total electrolytic process. Extensive research was conducted mostly over the NaF-AlF_3 melts in studying this process and yet there is a lot of space to fill in understanding it. In the initial stage of alumina addition in the melts, quick dissolution of alumina takes place. Alumina particles dissolve with the formation of activators due to the chemical reaction between the alumina and the melt. Alumina and cryolite crystallization takes place when the cold alumina is added to the hot melt and the pores of the alumina particles are penetrated leading to the rapid heat transfer between the melt and the particle. Gradually the alumina dissolution stabilizes, and after the saturation point, the equilibrium between the solid and dissolved species is reached [21].

In [22], the influence of the concentration of Al_2O_3 added to the NaF-AlF_3 melt and smelter grade alumina (SGA) particle size on the dissolution rate was determined. Findings show that with an increase in the alumina concentration, the dissolution time increases. the the larger the particle size, the faster it dissolves; γ-alumina has a higher dissolution rate than α-alumina. It has been stated that α-alumina does not go through phase transformation associated with the release of hydroxyls and low surface area associated with the gas dynamics resulting in the lack of interaction with the melts. Although, the alumina dissolution rate can be improved by preheating it at 600 °C [23]. Different results are obtained with CFD modelling. According to [24], the effective diffusion coefficient of dissolved alumina species increases with the increase in the alumina content in the melt making the dissolution process much easier for small alumina particles. The smaller alumina particle tends to dissolve within 10 s while the larger one takes more time. As mentioned earlier, alumina preheating can speed up the dissolution process. The alumina dissolution rate is independent of alumina content in the melt at alumina concentration C_A<3% while the dissolution rate decreases when C_A>3% because of the lack of free fluoride solvents in the sodium cryolite melts [8].

It is well known that the gas generation during the oxidation of carbon eliminates the agglomeration of alumina in the melt [25, 26]. The alumina-feeding rate has importance and plays a key role in avoiding the agglomeration of the alumina particles in the melt when fed [27]. Haverkamp et al. [28] proposed a diffusion model to calculate the dissolution rate of alumina. Dissolution rate W mainly depends upon the difference between the alumina saturation concentration (on the surface of the alumina) C_{sat} and current alumina concentration in the media C_A:

$$\boxed{W = \frac{dc}{dt}V = \frac{D}{\delta}A(C_{A(sat)} - C_A)} \quad (5)$$

where D is the diffusion coefficient, δ is the thickness of the boundary layer, t is the time.

The dissolution rate of alumina in acidic NaF-AlF_3 melts was investigated by Vasyunina et al. [29]. It was determined that

with a decrease in the cryolite ratio CR $\left(\frac{Mole\ \%\ NaF}{Mole\ \%\ AlF_3}\right)$ upon 1.8, the dissolution rate of alumina is drastically reduced. It was also found that the minimal dissolution rate ($2*10^{-3}$ wt %/s) of alumina required for the possibility of electrolysis in 300 kA cell can be only attained upon CR 1.8. The typical values obtained in the NaF-AlF3 melts with different CRs were in the range 1-6 $g{\cdot}kg^{-1}{\cdot}s^{-1}$ (20-120 $mole{\cdot}m^{-3}{\cdot}s^{-1}$), which are rather high in comparison with the results reported elsewhere [22].

Xiao et al. [30] investigated the solubility of alumina in NaCl-KCl based molten salts. It was found that in the melt with 1:1 wt.% of NaCl-KCl melt, there was no measurable solubility value. With the addition of additives AlF_3 → KF → Na_3AlF_6 → NaF (effect of additive on solubility in order), the solubility was improved to an acceptable limit. The temperature plays a key role in the functioning of the dissolution rate.

Hou et. al [31] conducted a numerical investigation to determine whether mass transfer mechanism or heat transfer mechanism predetermines the alumina dissolution at a given critical diameter of the particle. The studies suggest that particle size under 520 µm is controlled by a mass transfer mechanism while the particle size more than 520 µm is governed by a heat transfer mechanism.

Low-temperature electrolytes were studied in a narrow range of compositions, namely NaF-AlF_3 and KF-AlF_3 with CR=1.22 at 750 and 730 °C by Frazer et al. [10]. It was found that the alumina dissolution rate is higher in KF-based electrolytes. The same was observed by other researchers [32, 33]. It was also stated that alumina dissolution is a mass transfer-controlled process with the diffusion coefficient of dissolved alumina species D=1.8 – $2.2{\cdot}10^{-6}$ $cm^2{\cdot}s^{-1}$ at 750 °C, which is about five times lower than the values recorded at 960 °C.

It was reported in [32, 33] that an increase in KF content in the electrolyte from 2 to 7 wt.% leads to a 1.5 times increase in the dissolution rate. The values recorded at 950 °C were in the range of 0.4 – 0.7 $mole{\cdot}m^{-3}{\cdot}s^{-1}$. The dissolution rate depended on alumina concentration in the entire range of concentrations, which is in a contradiction with other results obtained with visual observation in a see-through cell [8]. The appearance of kinetic limitations at low alumina concentrations is a subject of further studies.

An increase in alumina concentration in the electrolyte from 0.5 to 3 wt.% at 950 °C results in a twofold drop in the dissolution rate. Even a small increase in temperature (up to 975 °C) leads to the threefold increase in the dissolution rate. It was also reported that it rises with CR of the electrolyte [32].

Isaeva et al. [34] studied the effects of alumina properties on the dissolution rate in commercial electrolytes. The reported values were as high as 0.05-0.075 $g{\cdot}kg^{-1}{\cdot}s^{-1}$ (1.0-1.5 $mole{\cdot}m^{-3}{\cdot}s^{-1}$)

The potentiometry studies of mechanically activated alumina were performed on the high-temperature commercial electrolyte by Yushkova et al. [35]. It was found that mechanical activation

leads to the 1.5 times higher dissolution rates under the same conditions. The initial rates were 0.014 and 0.022 $g \cdot kg^{-1} \cdot s^{-1}$ (0.28 and 0.44 $mole \cdot m^{-3} \cdot s^{-1}$) at 950 °C for non-activated and activated aluminas respectively, which is nonetheless lower than reported by other researchers [33]. The difference in dissolution rates obtained by different researchers shows that various methods lead to specific changes in the conditions. Visual observations can outline the general dependencies but the accurate measurement of the absolute values can be rather difficult as alumina particles may become transparent before they get dissolved. Despite the visual methods are widely used [8, 36-38] they perform better while used as additional with respect to instrumental electrochemical measurements.

The sedimentation behaviour of smelter grade alumina (SGA) suspension in KF-AlF_3 melts was studied previously [18, 19] at 700 °C and high alumina volume fractions (0.24-0.32). The Reynolds numbers for alumina sedimentation were in the range of $(7.88 \cdot 10^{-7})$-$(7.56 \cdot 10^{-3})$ that indicated the Stockesian regime. The values were significantly lower than those, calculated in [39] for both agglomerated and non-agglomerated alumina particles settling, which were in the range of 3.4-2545.8 for the size range from 40 μm (non-agglomerated) to 15 mm (agglomerated).

It was found in [18] that the sedimentation velocity decreases with an increase in particles volume fraction φ and reaches zero at maximum packing volume fraction being equal to 0.32 at 700 °C in the 1.3KF-AlF_3 melt. At φ=0.24 sedimentation velocity was as high as $9.7 \cdot 10^{-4}$ m s^{-1}.

This work complements the scarce data on dissolution and sedimentation kinetics in low-temperature melts and suspensions at different temperatures and melt (suspension) compositions. The topic challenges in Al production, which correlated with the presented paper are as follows:

- new environmentally friendly technologies are being developed;
- new technologies for producing high-purity aluminium are being developed;
- new high-amperage cells are being developed where the kinetics of alumina dissolution will be a more critical factor;
- new electrochemical technologies for the aluminium alloys production are being developed.

Experimental

Materials preparation

Electrolytes were synthesized at 900 °C from the dried individual chemically pure (p.a.) salts KF and AlF_3. Drying lasted for 4 hours at 400 °C. The prepared melt was purified from oxygen ions during 2 h electrolysis with a graphite anode under the potential of 1.5 V relative to the aluminium electrode potential. For dissolution and sedimentation studies 3 types of materials were chosen: smelter grade alumina (SGA) of Achinsk refinery, commercial α-Al_2O_3 (corundum) and mechanically activated (MA) alumina. The properties of the materials are presented in Table 1

Table 1. Materials properties

Material	Typical particle size, μm	BET-surface, $m^2 \cdot g^{-1}$	Content of α-modification	True density, $kg \cdot m^{-3}$	Reported dissolution rates
SGA	40-80	94	12	3630	Medium
MA alumina	1-10	60	12	3630	High
α-Al_2O_3	1-5	60	98	3950	Slow

Electrochemical measurements

The electrical conductivity κ_l of the molten cryolite is known to be decreased with the increase of the dissolved alumina concentration C_A. Different models described in [1] predict the value $\partial\kappa_l/\partial C_A \cong -0.05\,\Omega^{-1} \cdot cm^{-1} \cdot wt.\%^{-1}$. Addition of 1 wt.% of alumina will cause an appreciable change in cell resistance of 2.5-5 %. It makes possible to use the resistance-time dependence to estimate the alumina dissolution rate. The accurate technique to determine the resistance is electrochemical impedance spectroscopy (EIS). The resistance R of the electrochemical system is calculated out of impedance Z, given by the expression:

$$\boxed{\boldsymbol{Z = R - j \cdot \frac{1}{\omega \cdot C} = Z' - jZ''}} \quad (6)$$

where $j = \sqrt{-1}$, $Z' = R$ is the real part of the impedance, $Z'' = \frac{1}{\omega \cdot C}$ is the imaginary part of impedance, ω is the frequency of the AC polarization, C is the capacitance of the electrochemical system. The phase angle, φ, is given by the equation:

$$\boxed{\boldsymbol{tg\varphi = \frac{Z''}{Z'} = \frac{1}{R \cdot \omega \cdot C}}} \quad (7)$$

The EMF of the galvanic cell is given by the Nernst equation [21]:

$$\boxed{E^{rev} = E^0 - \frac{RT}{nF} ln \frac{a_O^{\upsilon_O}}{a_R^{\upsilon_R}}} \quad (8)$$

where E^0 is the standard EMF, a is the activity, υ is the stoichiometric coefficient, subindexes O and R denote oxidation and reduction forms.

If the activities of the species are unknown the EMF can be expressed as a function of dissolved alumina (for cryolite-alumina melts) concentration by the semi-empirical formula [41]:

$$\boxed{E^{rev} = -\frac{\Delta G^0}{6F} + \frac{RT}{6F} ln\left(\frac{C_{A(sat)}}{C_A}\right)^{2.77}} \quad (9)$$

where ΔG^0 is the change of Gibbs energy in the corresponding reaction.

For the concentration cell

$$C, CO_2 \,|\, KF\text{-}AlF_3,\ Al_2O_3(I) \,\|\, KF\text{-}AlF_3,\ Al_2O_3(II) \,|\, C, CO_2 \quad (10)$$

the EMF can be expressed by the equation:

$$\boxed{E^{rev} = \frac{RT}{6F} ln\left(\frac{C_{A(II)}}{C_{A(I)}}\right)^{2.77}} \quad (11)$$

where $C_{A(I)}$ and $C_{A(II)}$ are alumina concentration in the half-cells *I* and *II*.

The noted relations can be used for dissolution rate measurements if we measure EMF of the concentration cell as a function of time after addition of alumina into one of the half-cells.

After addition of excess (over the saturation value), alumina suspension is formed. The apparent electrical conductivity is known to be the function of the volume fraction of the dispersed phase. The Bruggeman equations describe this relationship for polydisperse particles of different irregular shapes [42]:

$$\boxed{\frac{\kappa_s}{\kappa_l} = (1-\varphi)^{3/2}} \quad (12)$$

where κ_s is the apparent conductivity of the suspension.

This model predicts the 8% decrease in cell resistance after a decrease in φ by 0.05 that is appreciably high value available for the measurement with the EIS technique. The change in resistance of the upper part of the cell during the sedimentation can be used to estimate the sedimentation velocity.

The electrochemical measurements were carried out in a two-electrode graphite cell heated by electrical furnace under air atmosphere in the temperature range of 750–850 °C. Two different experimental cells were used. The first one (Fig. 2a) was used with two electrochemical methods: electrochemical impedance spectroscopy (EIS) performed with frequency response analysis (FRA) at the galvanostatic mode in the range of 100-10000 Hz at the current amplitude of 10 mA; and open circuit potentiometry (OCP) with the concentration cell EMF measurement. The measurements were supported with visual observations. The second cell (Fig. 2b) was used for the critical current measurements at the linear sweep of the working electrode potential. The photo of the cell is shown in Fig. 3. The sweep was performed in the range of 1-10 V at the rate of 100 $V \cdot s^{-1}$. The temperature of the electrolyte was measured by the k-type thermocouple in a BN case connected to the controller and maintained constant (±2°C). The current and the potential were supplied or measured using Potentiostat AutoLab PGSTAT 302n and NOVA 2.1 Software (The MetrOhm, Netherlands). Both cells were placed inside the steel crucible compacted with graphite powder that is not shown in the figure.

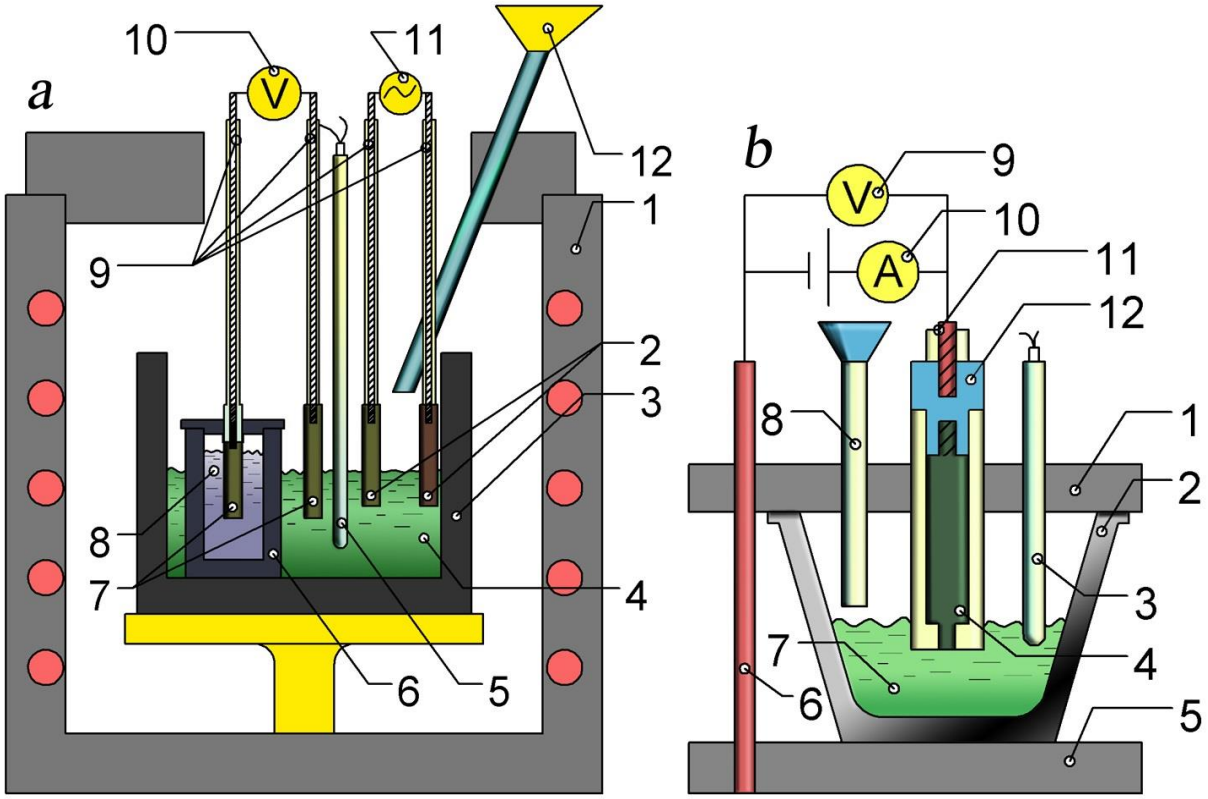

Fig. 2 – Schematic representation of experimental cells: a – a set up for coupled EIS and potentiometry methods (1 electrical furnace, 2 electrodes for AC polarization, 3 graphite vessel, 4 studied electrolyte (suspension), 5 thermocouple, 6 porous graphite crucible, 7 graphite electrodes for OCP, 8 electrolyte with the constant O^{2-} concentration, 9 current leads, 10 voltmeter, 11 potentiostat, 12 feeder); b – an electrochemical cell for linear sweep potentiometry (1 graphite cover, 2 glassy carbon vessel, 3 thermocouple, 4 graphite sensor, 5 graphite bottom, 6 cathodic current lead, 7 studied electrolyte, 8 feeder, 9,10 potentiostat, 11 anodic current lead, 12 steel connector

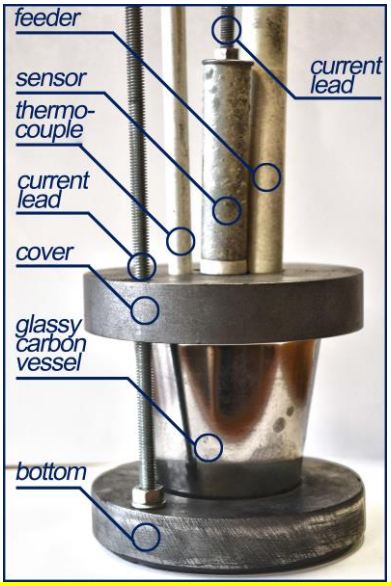

Fig. 3 – Photo of the cell for the linear sweep voltammetry

For the sedimentation study, the second half-cell was removed from the crucible. The suspension was mixed for one minute with a manual stirrer and after that EIS technique was continuously performed to record the resistance change in the upper part of the cell caused by the change in the solid particles local volume fraction.

The electrolyte samples were analyzed with the XRD technique to specify the composition.

Results and Discussion

Dissolution

The concentration cell EMF recorded during 15 minutes after addition of 2 g (1 wt.%) of SGA to the 1.3KF-AlF_3-Al_2O_3 melt at 750 °C was normalized with respect to the steady-state or quasi-steady-state value and presented in Fig. 4. Alumina feeding time was less than 1 s. The normalization was made to ease the comparison of the curves, which had different stationary EMF due to different alumina activities, and to eliminate the effects of the constant errors, which appeared due to the imperfections of the experimental procedure. The stationary potential difference E_{ss} was in the range of 10-35 mV depending on the concentration difference between two half-cells.

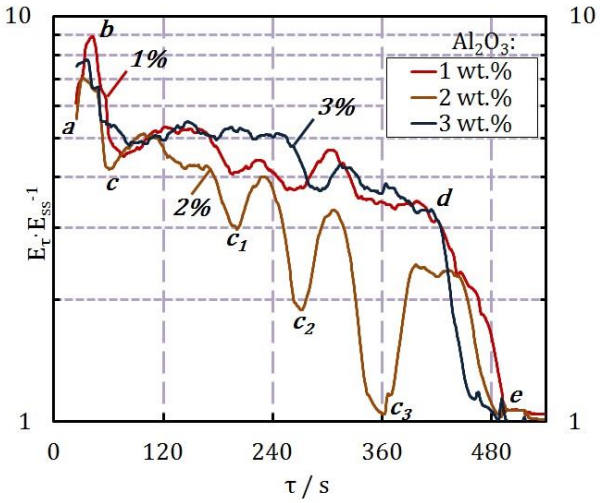

Fig. 4 – Dependence of normalized EMF of concentration cell (in log scale) vs. time for addition of 2 g of SGA to 200 g of 1.3KF-AlF_3 melt with 1-3 wt.% of dissolved alumina at 750 °C

The highest value of the concentration EMF was recorded to be 340 mV. The potential difference after the saturation of the studied melt was as high as 10-30 mV. It was higher than zero due to the slight difference in the ionic composition of the electrolytes in two half-cells and the diffusion potential at the porous membrane (asymmetry potential). The value of EMF decreased drastically during the first minutes after the addition of alumina (***ab*** region). The first peak ***abc*** can probably be explained by the heat effect of the addition of the cold sample, the crystallization and the melting of the electrolyte, the dissolution of the sample and the moisture evaporation. These effects did not depend on the concentration of O^{2-} ion in

the studied electrolyte. After two or more minutes the decrease of EMF was only due to the increase of oxygen ions concentration (region ***cd***). Between 120 and 240 s, the EMF decrease started after a different period of time, which is due to different hydrodynamic conditions caused the different durations of frozen electrolyte melting. The significant oscillations $E_\tau \cdot E_{ss}^{-1}$ were observed at the experiment with 2 wt.% of dissolved alumina (***c-c₁-c₂-c₃-d***). The nature of these oscillations is not clear.

The curves recorded at 1 and 3 wt.% had the drastic drop between 420 and 500 s after addition followed by the straight horizontal line indicated the equilibrium. The duration of the dissolution was 320, 360 and 220 s for 1, 2 and 3 wt.% of alumina respectively. These values give the dissolution rates as high as 0.031, 0.028 and 0.045 $g \cdot kg^{-1} \cdot s^{-1}$ (0.54, 0.48, and 0.78 $mole \cdot m^{-3} \cdot s^{-1}$) that is 2-4 times higher than normally reported for electrolytes based on sodium cryolite [22] The similar results were reported previously for NaF-KF-ALF_3 melts at 950°C [32, 33].

The typical Nyquist and Bode plots obtained with the EIS technique are presented in Fig. 5.

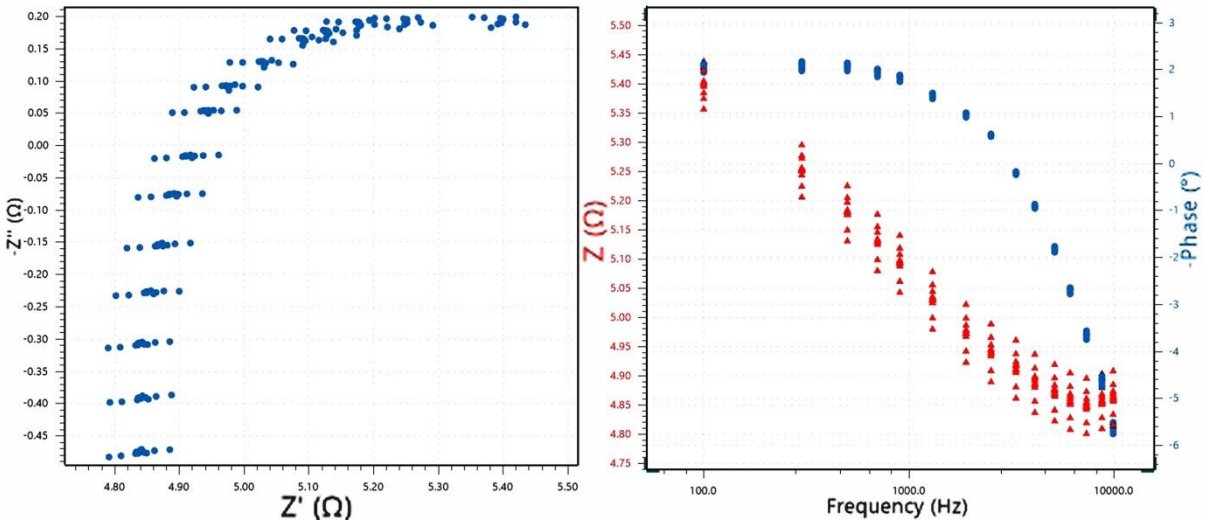

Fig. 5 – Nyquist plot –Z'' vs. Z' (left) and Bode plot for a set of measurements over the quasi-equilibrium molten 1.3KF-AlF_3 system at 750 °C

The effect of temperature on the dissolution kinetics at different concentration of O^{2-} ions is presented in Fig. 6 and 7.

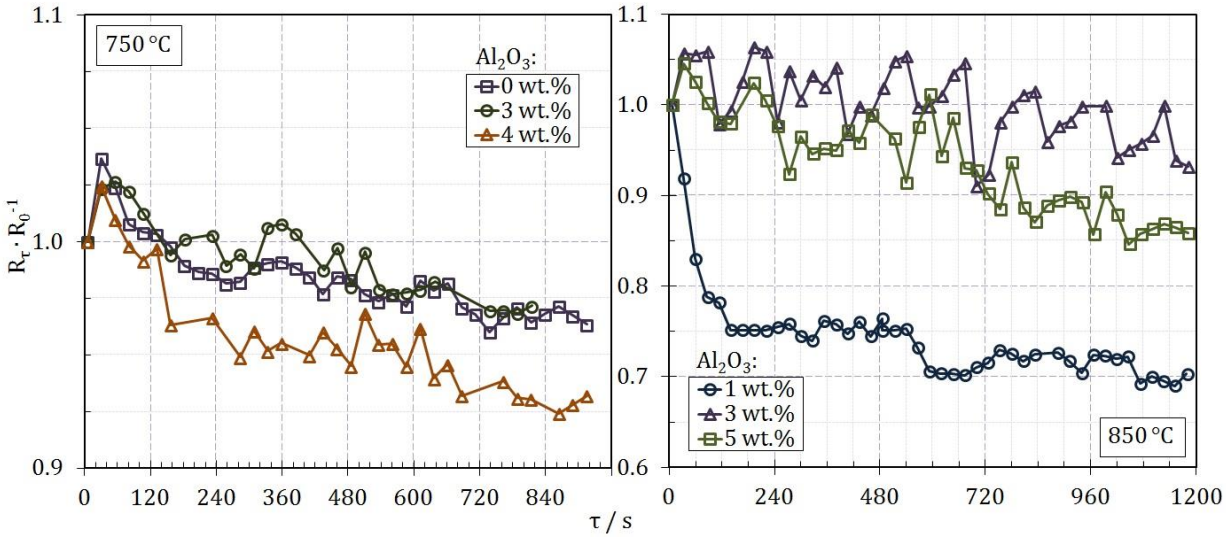

Fig. 6 – Dependence of normalized resistance vs. time for addition of 2 g of SGA to 200 g of 1.3KF-AlF_3 melt with 0-5 wt.% of dissolved alumina at 750 and 850 °C

The recorded resistance decreased with time after addition of SGA into the melt that is unlike the known data. The complex oxygen ions are known to decrease the electrical conductivity as well as a decrease in temperature due to the addition of the cold sample and its dissolution. The measured resistance was as high as 5.05Ω at the beginning of the set of experiments and decreased to 1.95Ω when the melt was saturated. The decrease was observed in 90% of experiments. The extremely high resistance could be caused by the interfacial passivation layers on the electrodes that were destroyed with an increase in dissolved alumina concentration.

In most cases, the short increase in resistance is observed during the first 30-50 s after addition. This phenomenon could be caused by the decrease in the temperature and solidification of the electrolyte with the increase of the solid phase volume fraction. After the peak of the curve is reached it starts to decrease and the initial slope is different for various alumina concentrations. The highest slope is observed for the low dissolved alumina concentrations at both temperatures. The end of the dissolution process is difficult to indicate on the curves. However, with the data obtained with OCP, it can be assumed that equilibrium is set between 360 and 500 s for different concentrations at 750 °C when the resistance is not decreased for an appreciable period of time (60 s or more).

The alumina dissolution at 850 °C lasts for less time. At C_A=1wt.% this process is finished 125 s after the addition. Growth of the concentration to 5 wt.% leads to an increase of dissolution time to 300 s.

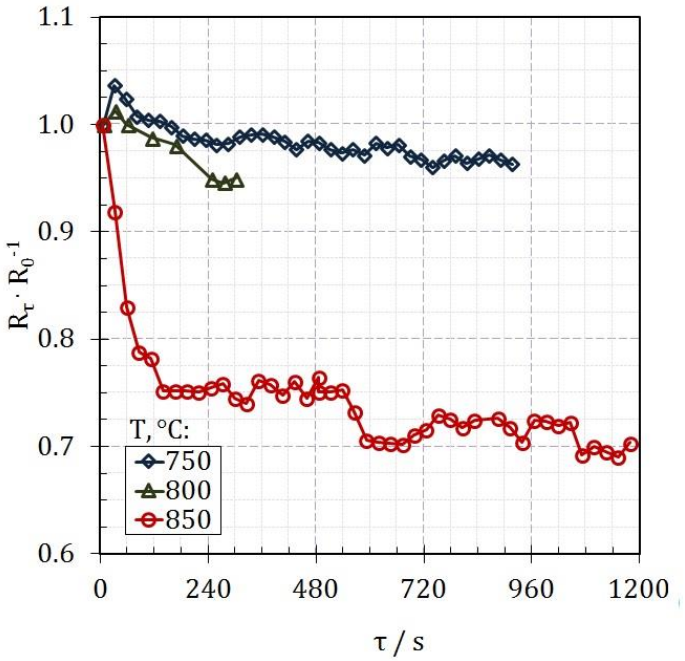

Fig. 7 – Dependence of normalized resistance vs. time for addition of 2 g of SGA to 200 g of 1.3KF-AlF_3 melt at 750, 800, 850 °C

The initial increase in the resistance, the rate of the further decrease and the time before reaching the equilibrium (or quasi-equilibrium) depend on the temperature. The dissolution rates (if it can be associated with the mentioned decrease) were as high as 0.023, 0.040 and 0.080 $g \cdot kg^{-1} \cdot s^{-1}$ at 750, 800 and 850 °C respectively. It means that an increase in temperature up to 50 ° double the dissolution rate. This is in agreement with previously obtained results reported in [32] for the NaF-KF-ALF_3 melt at 950-975 °C.

The second tested material was MA alumina, which is believed to increase the dissolution rate at low concentrations up to 2-4 times in comparison with SGA [35]. The normalized resistance and EMF of the concentration cell are placed on the same plots for dissolution of SGA and MA alumina in 1.3KF-AlF_3 (pure and 2 wt.% of alumina) at 800 °C (Fig. 8).

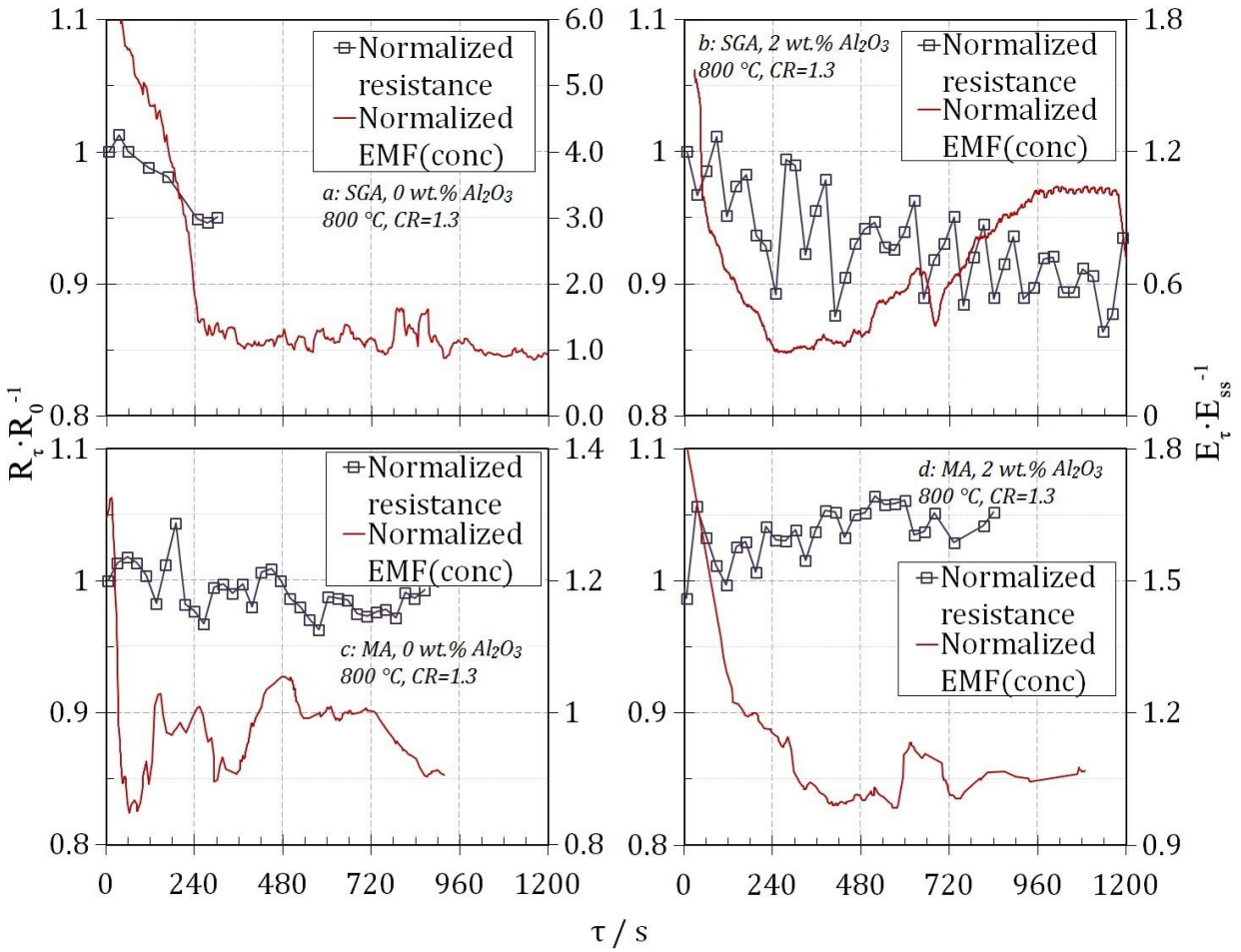

Fig. 8 – Dependence of normalized resistance and normalized EMF of concentration cell vs. time for addition of 2 g of SGA (a and b) or MA alumina (c and d) to 200 g of 1.3KF-AlF_3 melt with 0-2 wt.% of dissolved alumina at 800 °C

Addition of 2 g of SGA into KF-AlF_3 melt free of Al_2O_3 led to the decrease in both EMF and resistance during 240 s. Increase of the dissolved alumina concentration to 2 wt.% did not change this duration (according to the OCP). The resistance was oscillating that made the indication of the equilibrium difficult. After 2 minutes of the constant EMF between 240 and 360 s it started rising again with an increasing rate. The reason for that is might be the slow transfer of the electrolyte from one half-cell to another and change of the ionic composition.

The introduction of MA alumina into pure melt led to the fast dissolution during 60-70 s (which gives the dissolution rate 0.143-0.167 $g \cdot kg^{-1} \cdot s^{-1}$) according to the OCP technique results. The resistance of the cell was slightly increased during this time, after which the oscillation began to be observed. The increase in the alumina concentration to 2 wt.% led to the significant increase in the dissolution time up to 390 s. The reason for that can be the chemical reaction-controlled dissolution at low concentrations of dissolved alumina.

The change in concentration cell EMF after addition of α-Al_2O_3 with the particle size from 1 to 5 μm in 1.3KF-AlF_3 with

different content of aluminium oxide at 800 °C is presented in Fig. 9.

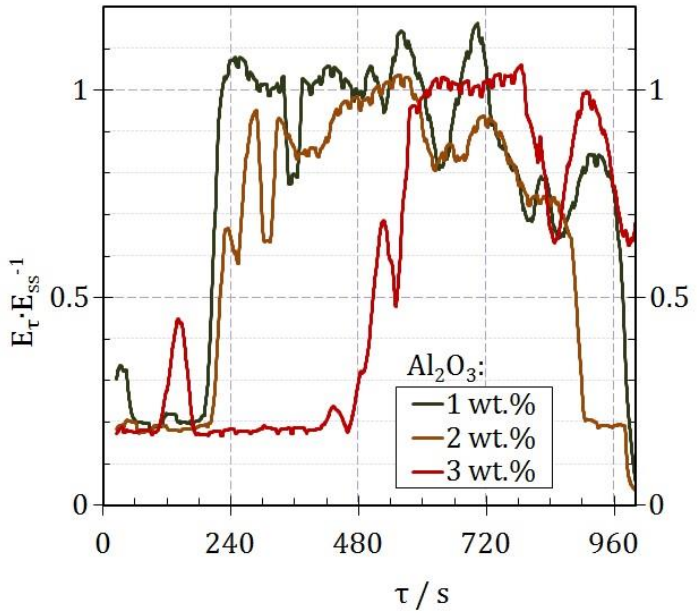

Fig. 9 – Dependence of normalized EMF of concentration cell vs. time for addition of 2 g of α-Al_2O_3 (1-5 μm) to 200 g of 1.3KF-AlF_3 melt with 1-3 wt.% of dissolved alumina at 800 °C

The introduction of α-Al_2O_3 had an effect different from ones of the previously studied materials. The curves were not changed significantly during the first 200-500 s. After this period of time (that depends on the oxide concentration) the drastic increase in EMF was followed. The resistance was oscillating. It is possible that α-Al_2O_3 had a long latency before the start of dissolution due to the surface inhabitation by the substance with low solubility. If the time of the EMF positive shift can be associated with dissolution time then dissolution rate can be calculated to be 0.167, 0.111 and 0.077 $g \cdot kg^{-1} \cdot s^{-1}$ at 1, 2 and 3 wt.% of dissolved oxide respectively.

Typical linear sweep voltammograms for dissolution of 2 g alumina portion in 200 g of electrolyte is displayed in Fig. 10. The peaks on the voltammograms are critical currents I_p connected with the concentration C_0 of O^{2-} ions by the expression [39]:

$$\boldsymbol{I_p = 0.28 \cdot n \cdot F \cdot A \cdot C_0 \cdot \sqrt{\pi \cdot D \cdot b}} \quad (13)$$

where

$$\boldsymbol{b = \frac{\alpha \cdot n \cdot F \cdot V}{R \cdot T}} \quad (14)$$

α is the transfer coefficient, n is the number of electrons participating in discharge, F is the Faraday constant, V is the potential sweep rate, R is the gas constant, T is the temperature (in Kelvin), A is the surface area of the electrode, D is the diffusion coefficient.

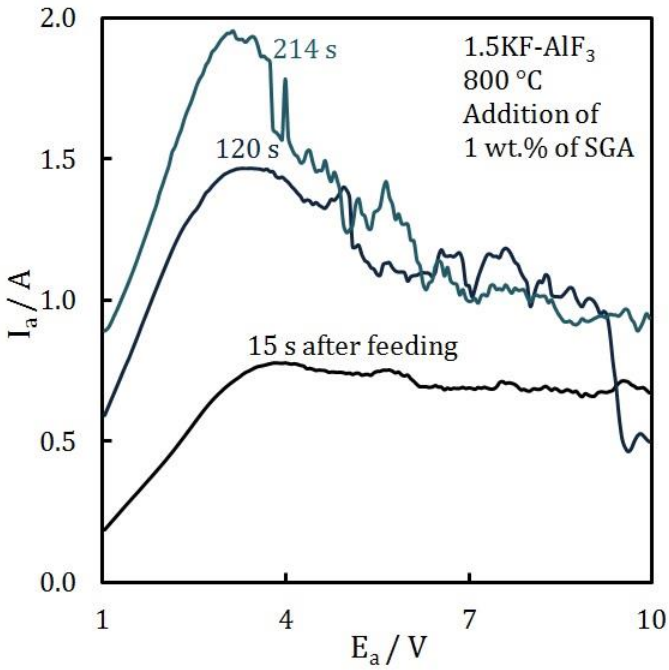

Fig. 10 – Dependence of peak current on linear sweep voltammograms recorded with 100 V s^{-1} at different times after addition of 2 g of SGA to 200 g of 1.5KF-AlF_3 melt with 0-2 wt.% of dissolved alumina at 800 °C

The equation (13) cannot be used for direct determination of the concentration due to the complicated hydrodynamic and diffusion conditions; however, the experimental data can be calibrated for the certain electrochemical system. The dependence between critical current vs. time can also be used to determine the dissolution rate.

The results of critical current measurement at potential sweep with the rate of 10 V·s^{-1} for anodic process on graphite in the 1.5KF-AlF_3 melt with different alumina concentrations for dissolution of SGA at 800 °C are shown in Fig. 11.

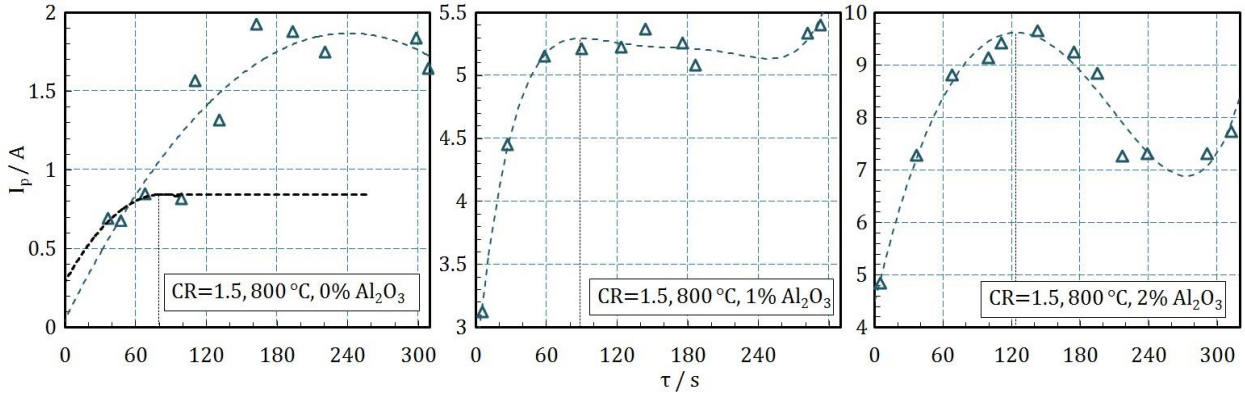

Fig. 11 – Dependence of peak current on linear sweep voltammograms vs. time for addition of 2 g of SGA to 200 g of 1.5KF-AlF_3 melt with 0-2 wt.% of dissolved alumina at 800 °C

The peak currents were increased with the time after addition of alumina to 1.5KF-AlF_3 melt. The first plateau is reached after 79 s in the pure melt. The second significant increase followed after the plateau and probably was due to

change in anode surface area. Increase of the alumina concentration to 1% led to an increase in the time before the plateau up to 90 s. At 2 wt.% of dissolved alumina, the dissolution time was 122 s, after which the appreciable drop followed. The calculated dissolution rates were 0.127, 0.111 and 0.082 $g \cdot kg^{-1} \cdot s^{-1}$ for 1, 2 and 3 wt.% of dissolved alumina respectively. All collected data presented in Table 2.

Table 2. Dissolution rates of different materials in KF-AlF_3 melt

No	Material	CR	T, °C	C_A, wt.%	W, $g/_{kg \cdot s}$	method
1	SGA	1.3	850	0	0.080	EIS
2	SGA	1.3	800	0	0.040	EIS
3	SGA	1.3	750	0	0.023	EIS
4	SGA	1.3	750	1	0.031	OCP
5	SGA	1.3	750	2	0.028	OCP
6	SGA	1.3	750	3	0.045	OCP
7	MA	1.3	800	0	0.143	OCP+EIS
8	α-Al_2O_3	1.3	800	1	0.167	OCP
9	α-Al_2O_3	1.3	800	2	0.111	OCP
10	α-Al_2O_3	1.3	800	3	0.077	OCP
11	SGA	1.5	800	1	0.127	LSP*
12	SGA	1.5	800	2	0.111	LSP
13	SGA	1.5	800	3	0.082	LSP

* LSP – linear sweep potentiometry

The dissolution rate measurements are highly difficult experimental procedures and the data obtained is sometimes difficult to be interpreted. We attempted to compare the results obtained with different techniques and in different conditions. The conclusions are questionable; however, some tendencies can be highlighted.

Dissolution rate depends on the ionic structure of the medium, so the increase in CR leads to the rise of the dissolution rate. This is in a good agreement with previous results for both low-melting and commercial electrolytes [3,6,32].

Dissolution rate depends on the dissolved alumina concentration in the melt at higher CR and temperature even at low concentrations (0-2 wt.%). At T=750 °C and CR=1.3, the dependence was not so clear. It is possible that CR and T highly affect the nature of rate-controlling stage. It is suggested that kinetic limitations at low alumina concentrations reported in [8] should be the subject of further work.

An increase in temperature naturally leads to the significant growth of the dissolution rate, which is in a good agreement with [32, 33]. Small particles (both α- and γ-alumina) dissolve more quickly than the large ones. It was previously reported [22, 34] that high content of fine particles reduces the dissolution rate due to the agglomeration mechanism. This was stated for the particle size less than 45 μm. In other paper [35] mechanically activated alumina with particle size less than 10 μm was sated to have a higher dissolution rate. In current work, alumina with size less than 5 μm was used. That means that dissolution rate may have a minimum at some certain alumina concentration value, which is suggested to be a subject of further study.

Mechanically activated particles are dissolved more quickly than SGA similarly to reported previously [35]; however, it is not clear whether this effect was due to the size of the particles or changes in the lattice. All three used methods give comparable results at similar conditions.

The findings allow us to conclude that in terms of dissolution rate the increase in temperature is preferable as well as using alumina with small particles and electrolytes with higher cryolite ratios. Mechanical activation can be considered for further investigation.

Sedimentation

The sedimentation velocity and the suspension stability are believed to be highly important parameters of novel electrolytes. The velocity U_{sp} of the single particle in the liquid is described by the Stokes equation:

$$\boxed{U_{sp} = \frac{2}{9} \cdot \frac{{a_p}^2 \cdot g \cdot (\rho_s - \rho_l)}{\eta}} \quad (15)$$

where a_p is the particle radius, g is the gravity acceleration, ρ is the density (subindexes s and l denote solid and liquid), η is the dynamic viscosity coefficient.

The collective (or batch) sedimentation velocity U_c is complicated by the $k(\varphi)$ function, which depends on the particles and medium properties and the suspension composition:

$$\boxed{U_c = \frac{1-\varphi}{k(\varphi)}} \quad (16)$$

The Reynolds number Re is an important hydrodynamic parameter that indicates Stokesian or non-Stokesian nature of sedimentation. It can be calculated according to the equation:

$$\boxed{Re = \frac{\rho_l \cdot U_c \cdot d_p}{\eta} = \frac{\rho_l \cdot Q \cdot d_p}{\eta \cdot S}} \quad (17)$$

where d_p is the particle diameter, Q is the volumetric flow rate, S is the channel surface area.

Both viscosity and density of liquid are the functions of the temperature so its effect on sedimentation velocity was studied with the EIS technique. The influence of the temperature on the sedimentation kinetics (indicated by the normalized resistance) of the suspension based on 1.3KF-AlF_3 melt with φ=0.1 is shown in Fig. 12

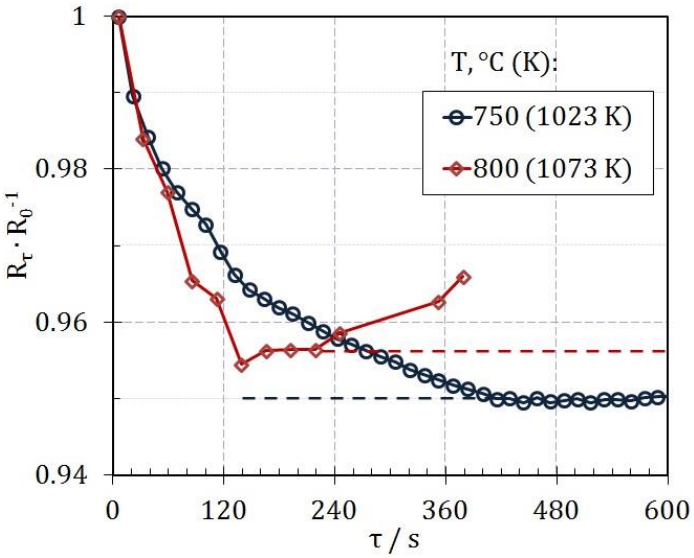

Fig. 12 – Dependence of normalized resistance vs. time for sedimentation in the 1.3KF-AlF_3-Al_2O_3(sat) suspension with 10 vol.% of solid alumina at 750 and 800 °C

It was observed that the resistance of the upper part of slurry in the cell started to decrease immediately after the stop of mixing that evidences the sedimentation of solid particles down the bottom part of the cell. The derivative $\partial R/\partial \tau$ can be associated with the sedimentation velocity according to the transformed equation (12):

$$\boxed{\frac{R_l}{R_s} = (1-\varphi)^{3/2}} \quad (18)$$

The initial value of $\partial R/\partial \tau$ seems to be the same at both temperatures till 40 s; however, the further changes in the resistance shows the differences in the sedimentation velocities. At both temperatures the sedimentation has two regimes changed after 90 s at 800 °C and 120 s at 750 °C. The quasi-steady-state resistance (and the solid particles local volume fraction in the upper part) was higher at high temperature due to the thermal convection and lower viscosity making the spontaneous mixing of the electrolyte easier. After reaching the quasi-steady-state the resistance started to increase again in 90-100 s that can be explained by uncontrollable fluctuations in the temperature, composition and surface properties of the electrodes and will not be considered further in this work. The volumetric flow rates for the first and the second regime were (1.92) and (0.36)·10^{-5} m^3/s at 750 °C; (3.47) and (0.64)·10^{-5} m^3/s at 800 °C. The corresponding Reynolds numbers were in the range of 0.006-0.022 that indicates the Stokesian regime of sedimentation.

The dependence between normalized resistance vs. time for the suspension with different aluminium oxides and different φ from 0.05 to 0.30 at 800 °C is presented in Fig. 13 and 14.

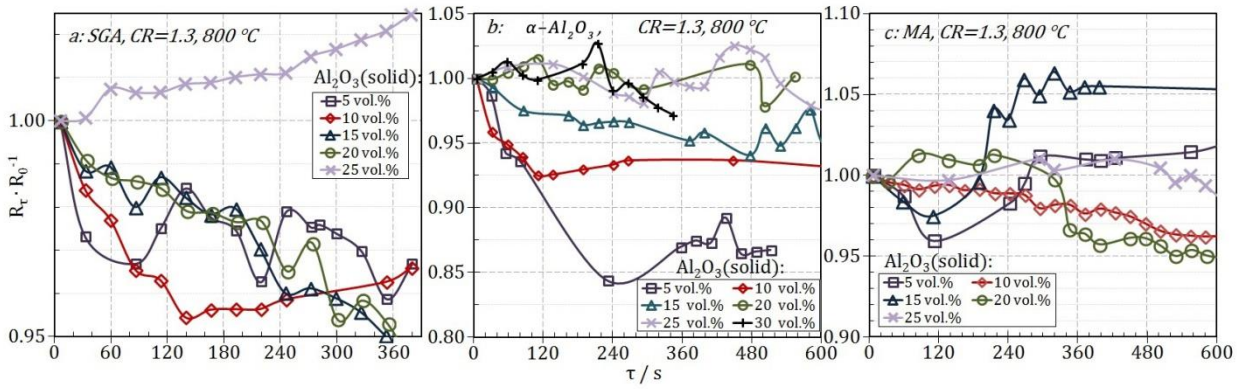

Fig. 13 – Dependence of normalized resistance vs. time for sedimentation of 1.3KF-AlF_3-Al_2O_3(sat) suspension with SGA (a), alpha aluminium oxide (b) and MA alumina (c) at 800 °C

Each studied material sedimented rapidly at low φ. The initial $\partial R/\partial \tau$ was the function of φ. Suspensions were stable even before maximum packing fraction φ_m, which was previously found to be around 0.32 [18]. Suspensions were stable or quasi-stable at φ equal to 0.25, 0.20 and 0.10 with SGA, α-Al_2O_3 and MA alumina respectively. The critical effect on the stability is caused by the particle size and the density of the particles.

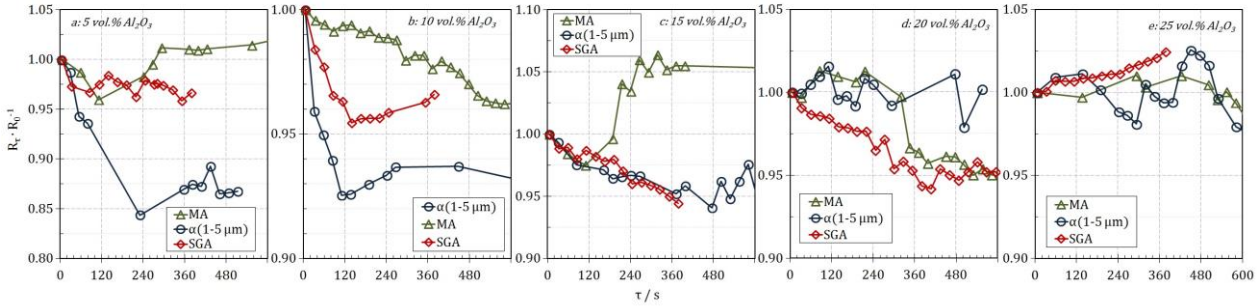

Fig. 14 – Dependence of normalized resistance vs. time for sedimentation of 1.3KF-AlF_3-Al_2O_3(sat) suspension with a-5, b-10, c-15, d-20 and e-25 vol.% of solid SGA, α-Al_2O_3 and MA alumina at 800 °C

At low φ the highest sedimentation velocity had dense α-Al_2O_3. At φ=*0.15* the sedimentation velocities were equal for all the studied materials. At φ>*0.15* the sedimentation velocities were higher for SGA due to the larger particle size. MA alumina had the best performance in terms of the suspension stability due to the low true density (in comparison with α-Al_2O_3), low particle sizes (in comparison with SGA) and probably modified surface caused by activation. All the collected data is presented in table 2.

Table 2. Sedimentation behaviour of different materials

No	*T*, °C	*Mat.*	φ	τ*, s	R_{ss}/R_0	φ_{up}	$Q \cdot 10^5$, $m^3 \cdot s^{-1}$	$U_c \cdot 10^2$, $m \cdot s^{-1}$	$Re \cdot 10^3$
1	750	SGA	0.10	1: 130	0.964	0.078	1.92	0.47	3.17
				2: 280	0.950	0.069	0.36	0.09	0.60
2	800	SGA	0.10	1: 70	0.965	0.078	3.47	0.85	5.96
				2: 90	0.957	0.073	0.64	0.16	1.10
3	800	SGA	0.05	1: 32	0.973	0.033	6.14	1.51	10.54
				2: 54	0.965	0.027	1.11	0.27	1.91

4	800	SGA	0.15	1: 32 2: 187	0.988 0.963	0.143 0.128	2.41 0.89	0.59 0.22	4.14 1.52
5	800	SGA	0.20	1: 60 2: 107	0.983 0.979	0.191 0.189	1.72 0.23	0.42 0.06	2.95 0.40
6	800	SGA	0.25	no	no	no	no	no	no
7	800	α-Al_2O_3	0.05	1: 29 2: 202	0.943 0.844	0.012 0.000	14.69 0.67	3.61 0.17	1.37 0.06
8	800	α-Al_2O_3	0.10	1: 31 2: 79	0.959 0.925	0.075 0.052	9.23 3.21	2.27 0.79	0.86 0.30
9	800	α-Al_2O_3	0.15	1: 84 2: 105	0.975 0.964	0.136 0.129	1.94 0.70	0.48 0.17	0.18 0.07
10	800	α-Al_2O_3	0.20	1: 32	0.999	0.199	0.19	0.05	0.02
11	800	MA	0.05	1: 59	0.987	0.042	1.59	0.39	0.27
12	800	MA	0.10	1: 59	0.994	0.096	0.69	0.17	0.12
13	800	MA	0.15	no	no	no	no	no	no

* duration of the sedimentation stage

The Reynolds number was in the range $(0.02\text{-}10.54)\cdot10^{-3}$, which indicates the Stokesian nature of sedimentation for all tested conditions. The sedimentation velocities were in the range $(0.06\text{-}3.61)\cdot10^{-3}$ $m\cdot s^{-1}$ that is several times higher than the values obtained previously [22] for lower temperature (700 °C) and higher particles volume fraction (0.24-0.32) by the pycnometric technique. The Reynolds number, as well as the sedimentation velocity, highly depends on the temperature, alumina volume fraction and properties. Both U_c and Re increase with T for both regimes of sedimentation due to a decrease in medium viscosity. The sedimentation is always 3-6 times more rapid during the first regime. The exception was the sedimentation of α-Al_2O_3 suspension with φ=0.05 where the first regime was 20 times more rapid than the second one.

The highest Reynolds numbers and velocities at φ=0.10 were demonstrated by the suspension with SGA for both regimes, while the lowest values were found for MA alumina. Moreover, a single regime could be distinguished for the sedimentation of MA alumina at any φ. The sedimentation stability of MA alumina can be reached at the lowest φ between 0.10 and 0.15. This allows us to conclude that in terms of sedimentation stability MA alumina is preferred material for industrial suspension-electrolyte. Lower temperatures are more beneficial for the reduction of sedimentation velocity, however, other limitations related to dissolution rate and electrode processes kinetics appear.

Conclusion

The effects of temperature, particle size and phase composition of the dispersed material and its volume fraction in the suspension on the dissolution kinetics and the sedimentation velocity are studied. It is shown that:

- typical alumina dissolution rates were in the range 0.028-0.167 $g\cdot kg^{-1}\cdot s^{-1}$, which is close to the values reported previously;
- an increase in the cryolite ratio leads to an increase in the alumina dissolution rate, which is in agreement with previously obtained data;

☐ the dissolution rate depends on the alumina concentration at higher cryolite ratios and temperatures even at low concentrations in the melt (0-2 wt.%). At T = 750 °C and CR = 1.3, the dependence is not so obvious, which suggests that CR and T can affect the nature of the rate-determining stage;

☐ mechanically activated particles dissolve faster than SGA, but it is not clear whether this effect is due to the particle size or changes in the crystal lattice;

☐ all three methods used to study the dissolution rate give comparable results under similar conditions; at the same time, measurements are technically difficult procedures, and the results are difficult to interpret;

☐ two consecutive sedimentation regimes can be distinguished, namely fast and slow. Sedimentation is usually 3-6 times faster during the first regime;

☐ the Reynolds number for sedimentation was in the range $(0.02\text{-}10.54)\cdot10^{-3}$, which indicates the Stokesian nature of sedimentation for all tested conditions and regimes;

☐ sedimentation velocities were in the range $(0.05\text{-}3.61)\cdot10^{-2}$ m/s, which is several times higher than the values obtained previously for 700 °C and φ = 0.24-0.32;

☐ the highest velocities and Reynolds numbers at φ=0.10 were demonstrated by a suspension with SGA for both regimes, while the lowest values were found for MA alumina. Moreover, only one regime (fast) can be distinguished for the sedimentation of MA alumina for any φ. The sedimentation stability of MA alumina can be achieved with the lowest φ between 0.10 and 0.15;

The use of alumina with fine particles and electrolytes with a higher cryolite ratio at 800 °C, as well as mechanical activation are the preferred solutions for the further development of the suspensions electrolysis technology. Given the limitations imposed by the cathodic process, the preferred cryolite ratio shall be 1.3-1.4. In this case, sedimentation stability can be achieved at φ=0.10...0.15.

Acknowledgements

The reported study was funded by RFBR according to the research project №19-38-50018.

References

1. Thonstad J., Fellner P., Haarberg G.M., Hives J., Kvande H., and Sterten A. (2001) Aluminium electrolysis. Fundamentals of the Hall-Heroult process. 3 ed. Dusseldorf, Aluminium-Verlag Marketing & Kommunikation GmbH, 354 p.

2. Galasiu I., Galasiu R., Thonstad J. (2007) Inert Anodes for Aluminium Electrolysis. Aluminium-Verlag, 2007, Diisseldorf, 207 p.

3. Thonstad J., Nordmo F., Paulsen J.B. (1972) Dissolution of Alumina in Molten Cryolite. METALLURGICAL AND MATERIALS TRANSACTIONS B, 3, (2), pp. 407–412.

4. Johnson A.R. (1982) Alumina crusting and dissolution in molten electrolyte. JOM, 34(3) pp. 63-68.

5. Picard G., Seon F. (1982). A molten salt potentiometric method for characterizing industrial aluminas. Electrochimica Acta, 27 (3), pp. 401-409.

6. Sum E., Skyllas-Kazacos M. (1989) Aluminium dissolution in the NaF-AlF_3-Al_2O_3 system: effects of alumina, temperature, gas bubbling and dissolved metal. JOURNAL OF APPLIED ELECTROCHEMISTRY, 19, pp. 485-494.

7. Haverkamp R.G., Welch B.J., and Metson J.B. (1992) Models of alumina dissolution in cryolite, Proc. Electrochemical Society, PV 1992-16, 646-659.

8. Yang Y., Gao B., Wang Z., Shi Z., Hu X. (2015) Effect of physiochemical properties and bath chemistry on alumina dissolution rate in cryolite electrolyte. JOM, 67 (5), pp. 973-983.

9. Thonstad J., Nordmo F., and Paulsen J. B. Dissolution of Alumina in Molten Cryolite. Metallurgical Transactions, 1972, 3, 403-408.

10. Frazer E.F., Thonstad J. (2010) Alumina solubility and diffusion coefficients of the dissolved alumina species in low-temperature fluoride electrolytes. METALLURGICAL AND MATERIALS TRANSACTIONS B, 41 (3), pp. 543–548.

11. Brown C.W. (2000) Laboratory experiments with low-temperature slurry-electrolyte alumina reduction cells, TMS Light metals, 391-396.

12. Brown C.W. (1998) The wettability of TiB_2-based cathodes in low-temperature slurry-electrolyte reduction cells, JOM, 50(5): 38-40.

13. Beck Th.R. (1994) Production of aluminium with low temperature fluoride melts, TMS Light Metals, 417-423.

14. Polyakov P.V., Klyuchantsev A.B., Yasinskiy A.S., and Popov Y.N. (2016) Conception of “Dream Cell” in aluminium electrolysis, TMS Light metals, 283-288.

15. Nikolaev A.Yu., Suzdaltsev A.V., Polyakov P.V., and Zaikov Yu.P. (2017) Cathode process at the electrolysis of KF-AlF_3-Al_2O_3 melts and suspensions, J. Electrochem. Soc., 164(8):H5315-H5321.

16. Yasinskiy A.S., Polyakov P.V., and Klyuchantsev A.B. (2017) Motion dynamics of anodic gas in the cryolite melt-alumina high-temperature slurry, Rus. J. Non-Ferrous Metals, 58(2):109-113.

17. Yasinskiy A.S., Vlasov A.A., Polyakov P.V., and Solopov I.V. (2016) Impact of alumina partial density on the process conditions of aluminium reduction from cryolite-alumina slurry parameters, Tsvetnye Metally, 2016(12):33-38.

18. Yasinskiy A.S., Polyakov P.V., Voyshel Y.V., Gilmanshina T.R., Padamata S.K. (2018), Sedimentation behaviour of high-temperature concentrated colloidal suspension based on potassium cryolite, J. Dispersion Sci. & Tech., 39:1492-1501.

19. Yasinskiy A.S., Polyakov P.V., Yushkova O.V., Sigov V.A. Spatial particle distribution during stokes sedimentation of alumina in high temperature concentrated suspension-electrolyte for aluminium production. Tsvetnye Metally, 2018, 2, pp. 45–50.

20. Yasinskiy A.S., Padamata S.K., Polyakov P.V., Vinogradov O.O. (2019) Anodic process on aluminium bronze in low-temperature cryolite-alumina melts and suspensions. Tsvetnye Metally, 9, 42-49.
21. Kan H., Zhang N., Wang X. (2012) Dissolution rate determination of alumina in molten cryolite-based aluminium electrolyte. Journal of Central South University, 19, 897-902.
22. Issaeva L.A., Poliakov P.V., B'linov V.A., Mikhalev Iou.G., Buzunov V.I. (1998) Rates Of Dissolution Of Commercial Aluminas With Different Physical Properties. Light Metals, 508-512.
23. Lavoie P., Taylor M.P., and Metson J.B. (2016) A Review of Alumina Feeding and Dissolution Factors in Aluminium Reduction Cells. Metallurgical and Materials Transactions B, 47(4), 2690-2696.
24. Zhan S., Li M. , Zhou J., Yang J., Zhou Y. (2014) CFD simulation of dissolution process of alumina in an aluminium reduction cell with two-particle phase population balance model. Applied Thermal Engineering, 73, 803-816.
25. Sum E., Skyllas-Kazacos M. (1989) Aluminium dissolution in the $NaF-AlF_3-Al_2O_3$ system: effects of alumina, temperature, gas bubbling and dissolved metal. Journal Of Applied Electrochemistry, 19, 485-494.
26. Yang Y., Gao B., Wang Z., Shi Z., and Hu X. (2013) Mechanism of Dissolution Behaviour of the Secondary Alumina. Metallurgical And Materials Transactions B, 44(5), 1296-1303.
27. Tessier J., Cantin K., and Magnusson D.T. (2018) Investigation of Alumina Concentration Gradients within Hall-Héroult Electrolytic Bath. The Minerals, Metals & Materials Series: Light Metals, 515-522.
28. Haverkamp R.G., and Welsh B.J. (1997) Modelling the dissolution of alumina powder in cryolite, Chemical Engineering and processing, 37, 177-187.
29. Vasyunina N.V., Vasyunina I.P., Mikhalev Yu.G., and Vinogradov A.M. (2009) The Solubility and Dissolution Rate of Alumina in Acidic Cryolite Aluminous Melts. Russian Journal of Non-Ferrous Metals, 50 (4), 338-342.
30. Xiao Y., Tang K. (2009) Chapter 5: "Solubility of Alumina in Molten Chloride-Fluoride Melts. Molten, 1393-1401.
31. Hou W., Li H., Li M., Zhang B., Wang Y., Gao Y. (2019) Multi-physical field coupling numerical investigation of alumina dissolution. Applied Mathematical Modelling, 67, 588-604.
32. Apisarov A. (2007) Influence of the cation composition on the physical and chemical properties of melts for electrolytic production of aluminium. CSc thesis, Institute of High-Temperature Electrochemistry UB RAS, Yekaterinburg [In Russ], 108.
33. Frolov A., Gusev A., Zaikov Yu., Khramov A., Shurov N., Tkacheva O., Apisarov A., Kovrov V. (2007) Modified alumina-cryolite bath with high electrical conductivity and dissolution rate of alumina. Light metals, 571-576.
34. Isaeva L.A., Braslavskii A.B., Polyakov P.V. (2009) Effect of the content of the α-Phase and granulometric

composition on the dissolution rate of alumina in cryolite-alumina melts. Russian journal of non-ferrous metals, 50, 600-605.

35. Yushkova O.V. Isaeva L.A., Polyakov P.V., Avvakumov E.G. (2018) The influence of mechanical activation on the dust index and the dissolution rate of alumina in the molten cryolite. Tsvetye metally, 8, pp. 63-68.

36. Yang Z., Gao B., Xu N., Qiu Z., Liu Y. (1999) Dissolution of Alumina in Molten Cryolite: A Video Recording Study. Journal of Northeastern University (Natural Science), 20(4), 398–400.

37. Xu J., Shi Z., Gao B., Qiu Z. Dissolution of Alumina in Molten Cryolite. Journal of Northeastern University (Natural Science), 2003, 24(9), 832–834.

38. Fan L., Qiu Z., Grjotheim K. (1986) A direct observation of the process of aluminium in cryolite-alumina electrolyte through a transparent quartz cell. Journal of Northeastern University, 46(1), 97–106.

39. Zhan S., Li M., Zhou J., Yang J., Zhou Y. (2015) Analysis and modelling of alumina dissolution based on heat and mass transfer. Transactions of nonferrous metals society of China, 25, 1648-1656.

40. Bard A.J., Faulkner L.R. (2001) Electrochemical methods. Fundamentals and Applications. Second edition, John Wiley & sons, inc., 833.

41. Grjotheim K., Kvande H. (1993) Introduction to Aluminium Electrolysis. Understanding the Hall-Heroult Process. 2nd edition. Aluminium-Verlag, Dusseldorf, 212.

42. Padamata S.K., Yasinskiy A.S., Polyakov P.V. (2019) Electrolytes and its Additives Used in Aluminium Reduction Cell: a Review. Metallurgical research and technology, 116 (4), 410.